Journal of Alloys and Compounds 509 (2011) 5230–5237

Contents lists available at ScienceDirect

Journal of Alloys and Compounds

journal homepage: www.elsevier.com/locate/jallcom

Ab initio electronic structure calculations and optical properties of ordered and disordered Ni_3Al

Altaf Hussain[a,*], Sitaram Aryal[b], Paul Rulis[b], M. Arshad Choudhry[a], Jun Chen[c], W.Y. Ching[b]

[a] Department of Physics, The Islamia University of Bahawalpur, Punjab 63100, Pakistan
[b] Department of Physics, University of Missouri-Kansas City, MO 64110, USA
[c] Institute of Applied Physics and Computational Mathematics, Beijing 10088, China

ARTICLE INFO

Article history:
Received 30 July 2010
Received in revised form 10 February 2011
Accepted 15 February 2011
Available online 22 February 2011

Keywords:
Density functional
Electronic structure
Optical properties
Nickel aluminides
Intermetallic compounds

ABSTRACT

The electronic structure and optical properties of the Ni_3Al intermetallic alloy are studied by the first-principles orthogonalized linear combination of atomic orbitals method. Disordered models at different temperatures were constructed using molecular dynamics and the Vienna *ab initio* simulation package. The average charge transfer from Al to Ni increases steadily with temperature until the liquid phase is reached. The localization index shows the presence of relatively localized states even above the Fermi level in the disordered models. The calculated optical conductivity of the ordered phase is rich in structures and in reasonable agreement with the experimental data. The spectra of the disordered Ni_3Al models show a single broadened peak at 4.96 eV in the 0 K model which shifts towards 6.62 eV at 1400 K and then down to 5.83 eV in the liquid phase. Other results on the band structure and density of states are also discussed.

1. Introduction

The development of intermetallic alloys for structural applications has been an active field of research around the world for the last three decades. A sampling of the research results have been published in many books [1–3], conference proceedings [4–8], and journal articles [9–11]. Most of the research effort has been concerned with Ni_3Al, NiAl, Ni_3Si, Fe_3Al, FeAl, Ti_3Al, TiAl, and $MoSi_2$. Strength at high-temperatures and superior oxidation resistance make intermetallic materials exceptional candidates for use in component design where long service life in a hostile environment is required. Promising applications include heat treating fixtures, transfer rolls for hot metal processing, forging dies, radiant burner tubes, or pyrolyzer parts [12–15]. Among the most investigated of the various intermetallics are the nickel aluminides. They possess advantageous properties such as: high tensile strength and yield point, low density, high-temperature creep resistance and good corrosion resistance at elevated temperatures [16–20]. In particular, Ni_3Al has been a subject of continuous interest because of its simple structure, attractive mechanical properties, and relatively inexpensive constituent elements. The flow strength of this intermetallic alloy shows an anomalous increase at relatively high-temperatures [21]. Experimental studies performed on Ni_3Al have considered the magnetic properties [22], magnetic field effects on heat capacity [23], neutron scattering [24], de Haas-van Alphen (dHvA) effect [25], elastic constants [26], and optical properties [27–30]. Among its various physical properties, the optical conductivity is the most controversial [29]. The major controversy lies in the vastly different positions and magnitudes of the peaks structures of both the measured and calculated results. Such differences could root from different methods of preparation of the samples, different nature of the samples' surfaces, different energy ranges studied, and different methods of calculation used to perform theoretical calculations.

Experimentally the optical conductivity (σ) of the ordered ($L1_2$) Ni_3Al has been measured using ellipsometry [27–30]. In 1985 Van der Heide et al. [27] measured σ from 0.5 to 5.3 eV at room temperature under ultra-high vacuum conditions using single crystal and polycrystalline samples. They observed a large, broad peak centered at 4.32 eV and a small shoulder starting at 0.72 eV ending at 1.10 eV. Rhee et al. in 1997 [28] reported a single broad peak in their measured σ spectrum around 4.4 eV and concluded that the main contribution to this peak comes from the transitions at k-points close to the Γ–M–R plane. Their σ was almost 50% larger than that of Van der Heide et al. [27]. The authors hypothesized that this discrepancy was due to the rough overlayer of the sample used in previous studies. Again in 2003 Rhee et al. [29] investigated the optical properties of two γ' phases of Ni_3Al ($Ni_{0.752}Al_{0.248}$ and $Ni_{0.771}Al_{0.229}$). Two intense interband absorption features at ~0.8 eV and ~4.2 eV were observed. The new peak at ~0.8 eV was

* Corresponding author. Tel.: +92 321 6823467; fax: +92 062 925 5519.
E-mail address: altafiub@yahoo.com (A. Hussain).

0925-8388/$ – see front matter © 2011 Elsevier B.V. All rights reserved.
doi:10.1016/j.jallcom.2011.02.071

not present in their previous work [28]. More recently Hsu et al. [30] measured the σ of polycrystalline Ni_3Al in the 0.6–4.0 eV energy range. They observed a peak-like structure at 0.89 eV and a shoulder at 1.27 eV at room temperature.

On the theoretical side, there were three key studies performed on the ordered phase of this alloy [27,28,31]. In Ref. [27], the authors used a self-consistent augmented-spherical-wave (ASW) method in their calculations without the inclusion of the dipole transition matrix (DTM) elements. Their theoretical curve showed two peaks at 3.4 and 3.9 eV. To ascertain the effects of the DTM elements, Khan et al. [31] calculated the σ curve using a linear-muffin-tin-orbital (LMTO) method within the atomic sphere approximation (ASA). They found that matrix elements play a significant role in influencing the magnitude of σ and the position of peaks. However, spin-orbit coupling was not included in this study. Later on, Rhee et al. [28] included the DTM elements and spin-orbit coupling in order to fit to their measured σ data in the range of 1.5–5.4 eV. In these theoretical calculations the authors claimed to observe the peaks at different positions and there was even disagreement about the number of peaks observed. Moreover the energy range considered was also short. This invites a further, more comprehensive, study to provide information to resolve this issue.

For disordered Ni_3Al, most of the previous work focused on the effects of milling parameters on its synthesis [32], the vibrational thermodynamics and entropy of disordered alloys [33,34], transmission electron microscopy (TEM) observation of the reordering mechanism [35], phonon DOS, and ordering kinetics [36,37]. To the best of our knowledge, no experimental measurements or theoretical calculations on the electronic structure and optical properties of the disordered phase of Ni_3Al have been reported. In view of the diverse nature of the results for the ordered phase and the total absence of any investigation on the disordered phase, a more comprehensive study on both phases are necessary. In this paper we report the results of theoretical calculations on both ordered and disordered phases of Ni_3Al using the first-principles orthogonalized linear combination of atomic orbitals (OLCAO) method within the local density approximation (LDA) of the density functional theory (DFT) [38]. No attempt is made to go beyond the LDA theory for optical properties calculations although we are aware of recent developments such as time dependent DFT and more rigorous theories that account for many electron effects which have been applied to simple crystals. We also calculate the localization index (LI) of the electron states and effective charges (Q^*) on Ni and Al, thereby providing additional understanding of the alloy and the charge transfer effects that influence its energetics [39].

The paper is organized as follows: in Section 2, we describe the method of calculation. The results on the electronic structure and optical properties of the ordered phase of Ni_3Al are presented in Section 3. In Section 4, we report the results of the disordered phase modeled at various temperatures. The paper ends by describing the major conclusions of the work presented.

2. Methodology

In the OLCAO method, the basis functions used for the construction of Bloch functions are atomic orbitals. This is a well-established all-electron method that has been used successfully to study many crystal systems and various properties [40–44]. The atomic orbital basis is most useful for the interpretation of results, especially in the form of effective charges (Q^*) on each atom, and the atom-, orbital-, or spin-resolved partial density of states (PDOS). Different types of basis functions are used in the OLCAO method. A full basis (FB)–which consists of the core orbitals, the valence shell orbitals, and one additional shell of atomic orbitals for each atom–is used mainly for the self-consistent field calculation of the crystal potential. A minimal basis (MB) set is used for Q^* calculations using the Mulliken population analysis scheme [45], which is most effective when the basis functions are more localized. As an example, the MB set of Ni consists of the 1s, 2s, 2p, 3s, 3p, 3d, and 4s orbitals, the FB has 4p, 4d, and 5s added to it. In the electronic structure and optical properties calculations, we used the FB set. Self-consistency is achieved by an iterative process. We used 364 (35) k-points in the irreducible portion of the Brillouin zone (BZ) for the ordered Ni_3Al primitive cell ($4\times4\times4$ supercell) calculations, while for disordered phase calculation at different temperatures, we used 27 k-points. An experimental lattice constant of 3.568 Å [28] was used in our calculations as the initial value for the ordered as well as the disordered phase of Ni_3Al.

The LI (L_m) for the state m is an approximate measure of the spread of the wave function of the electron state and is particularly useful for identifying the degree of disorder in amorphous systems. Mathematically, LI is calculated as:

$$L_m = \sum_{i,\alpha} [\rho_{i\alpha}^m]^2 \tag{1}$$

where $\rho_{i\alpha}^m$ is the fractional electron charge assigned to the αth atom and is calculated from the resulting eigen functions as:

$$\rho_{i\alpha}^m = \sum_{j,\beta} C_{i\alpha}^{m^*} C_{j\beta}^m S_{i\alpha,j\beta} \tag{2}$$

where $C_{j\beta}^m$ are the eigenvector coefficients, $S_{i\alpha,j\beta}$ the overlap integrals, m the band index, i and j the atomic orbitals, and α and β the atomic labels. L_m lies between $1/N$ for a completely delocalized state and 1 for a completely localized state in which charge is confined to a single orbital (N is the dimension of the Secular equation, or the total number of states of the system). Further details of the OLCAO method have been previously published [38,45].

The effective charge Q_α^* based on the Mulliken scheme [46] of molecular orbital theory, is defined as the valence electrons associated with an atom α in the crystal and is calculated as:

$$Q_\alpha^* = \sum_i \sum_{n,occ} \sum_{j,\beta} C_{i\alpha}^{*n} C_{j\beta}^n S_{i\alpha,j\beta} \tag{3}$$

Q_α^* also provides information about charge transfer. This number is always positive and should not be confused with the valence charge state.

The interband optical conductivity σ is an important physical observable which can be directly compared with experimental data. In the OLCAO approach, the real part of the interband optical conductivity $\sigma(\hbar\omega)$ is calculated in the random phase approximation (RPA) using the Kubo–Greenwood formula [47]:

$$\sigma(\hbar\omega) = \frac{e^2}{4\pi^2 m\omega} \times \int \mathrm{d}\vec{k} \sum_{n,l} \left| \langle \psi_n(\vec{k},\vec{r}) \right| \vec{P} \left| \psi_l(\vec{k},\vec{r}) \rangle \right|^2 \times f_l(\vec{k})[1-f_n(\vec{k})]\delta(E_n(\vec{k}) - E_l(\vec{k}) - \hbar\omega) \tag{4}$$

where $E=\hbar\omega$ is the photon energy, $f(\vec{k})$ is the Fermi distribution function, and l labels an occupied state and n an unoccupied state. $\langle \psi_n(\vec{k},\vec{r}) \left| \vec{P} \right| \psi_l(\vec{k},\vec{r}) \rangle$ is the momentum matrix element (MME).

3. Results of the ordered phase

The ordered Ni_3Al exists in the simple cubic Cu_3Au structure with Ni atoms at the face centers and Al atoms at the corners of the cube as shown in Fig. 1(a). The *Strukturbericht* designation for this compound is $L1_2$ with space group $Pm\bar{3}m$ (No. 221). Fig. 2 shows the calculated band structure of Ni_3Al along select high symmetry directions. This band structure is very similar to those of Rhee et al. [28], and Khan et al. [31].

Fig. 3(a) shows the calculated total DOS (TDOS) and atom-resolved partial DOS (PDOS) for Ni_3Al. The TDOS is dominated by the Ni-3d states, while the contribution from Al is small. The major peak in the TDOS is at −0.93 eV below the Fermi level (E_F). The E_F is on the steep side of the Ni-3d peak, resulting in a d-band hole. The

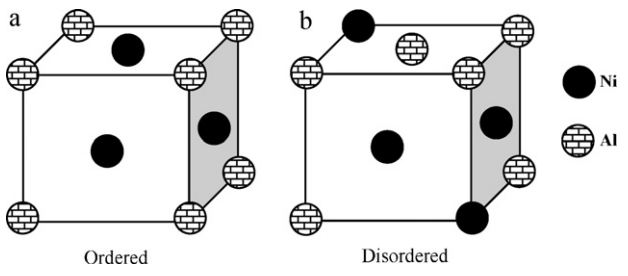

Fig. 1. Unit cell representation of Ni_3Al alloy (a) ordered phase, and (b) disordered phase. In disordered alloy Ni and Al atoms occupy random positions.

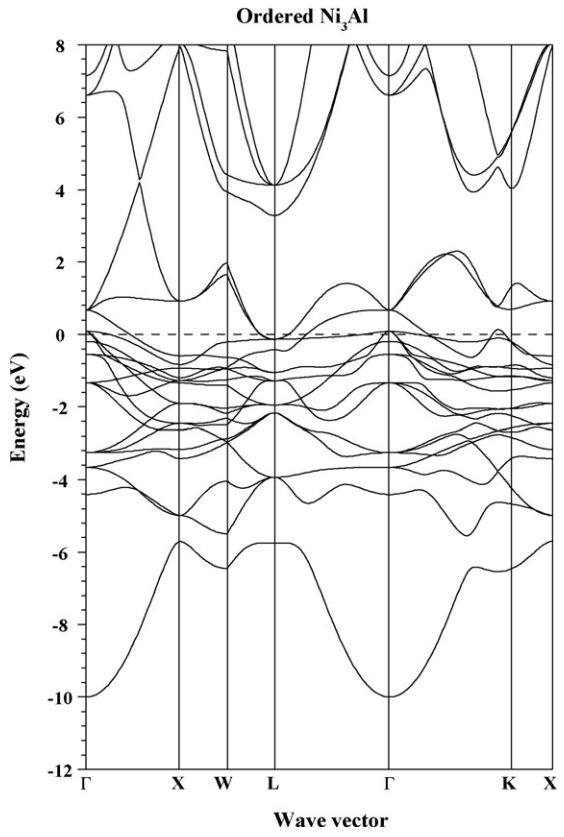

Fig. 2. Band structure of ordered Ni_3Al in Cu_3Au structure along high-symmetry lines. Dotted line represents the Fermi level ($E_F = 0$ eV).

total DOS at E_F, $N(E_F)$, is 5.77 states/(eV formula unit), mostly from Ni (5.54 states/(eV formula unit)) and less from Al (0.23 states/(eV formula unit)).

In order to be able to account for the intraband optical transitions in the conductivity calculations, we repeated the above calculation using a supercell approach. The supercell is constructed from suitable repetitions of the primitive cell. The supercell contains a much larger number of atoms per cell but the corresponding BZ is much smaller, hence fewer *k*-points are needed. The bands

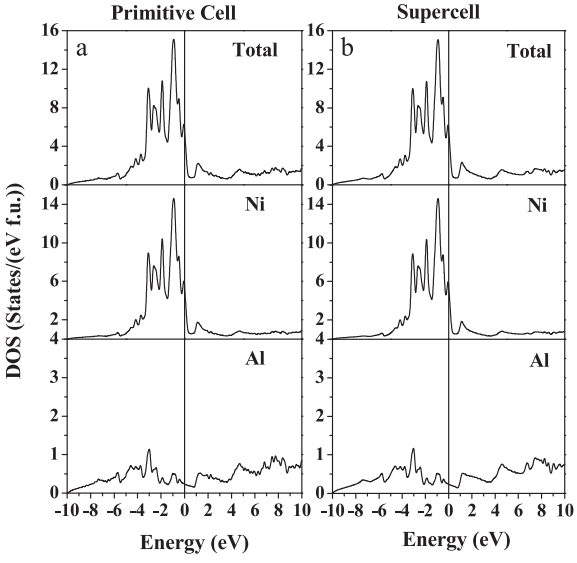

Fig. 3. Total and partial DOS plots for ordered Ni_3Al using (a) primitive cell and (b) supercell calculations. The Fermi level is taken as zero energy.

Table 1
Effective charge (Q^*) data for ordered and disordered phases of Ni_3Al.

		Mean Q^*	Max Q^*	ΔQ^*
Ordered				
	Ni	10.156	10.165	+0.156
	Al	2.539	2.539	−0.461
Disordered				
0 K	Ni	10.123	10.505	+0.123
	Al	2.615	2.743	−0.385
300 K	Ni	10.141	12.244	+0.141
	Al	2.576	3.923	−0.424
1000 K	Ni	10.144	12.448	+0.144
	Al	2.567	3.954	−0.433
1400 K	Ni	10.156	12.431	+0.156
	Al	2.533	3.753	−0.467
1800 K	Ni	10.130	11.976	+0.130
	Al	2.610	3.749	−0.390

in the primitive cell (Fig. 1(a)) calculation are folded into multiple bands in the reduced BZ of the supercell such that "interband transitions" in the reduced BZ account for the intraband transitions in the regular BZ. In the limit of an infinitely large supercell, all intraband transitions are included. For amorphous solids or disordered alloys, a supercell description of the structure is the only option since the system is no longer periodic and, strictly speaking, the Bloch theorem no longer holds. In the present case for Ni_3Al a $4 \times 4 \times 4$ supercell with 256-atoms is used. Fig. 3(b) shows the calculated TDOS and PDOS of ordered Ni_3Al from the supercell calculation. The results reproduce those of the primitive cell calculation.

The calculated Q^* data are listed in Table 1. A net charge transfer from Al to Ni atoms is shown. Ni atoms gain a charge of 0.156 electrons/atom on average, while the Al atoms lose an average of 0.461 electrons/atom. The average values of Q^* for Ni and Al are 10.156 and 2.539 electrons, respectively. It should be emphasized that the Q^* calculation for a metallic system is only used for a qualitative estimate. In metallic systems, the electron wave functions are quite extended while Q^* calculations based on Mulliken scheme using a MB set, which is relatively localized.

The calculated optical conductivity of ordered Ni_3Al using a supercell is shown in Fig. 4. Also shown are the experimental data of Rhee et al. [29] and Hsu et al. [30]. The data from Ref. [30] has a much larger amplitude compared to the calculated one and that of Ref. [20] probably because of the polycrystalline nature of the sample which has a 2–3% Ni deficiency. The calculated σ shows three prominent peaks B, C, and D at 1.46, 4.21, and 5.40 eV, respectively, and two less prominent features A and A′ on either side of the peak

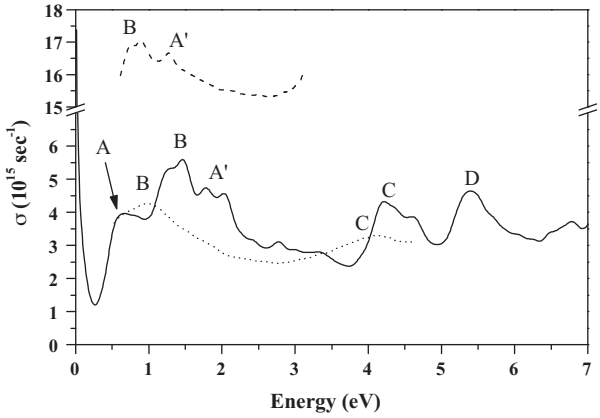

Fig. 4. Optical conductivity spectra for ordered ($L1_2$) Ni_3Al alloy. Solid line represents our calculated results while the experimental data from Refs. [29,30] has been shown by dotted and dashed lines, respectively.

B at 0.63 and 1.91 eV, respectively. Experimental data by Hsu et al. [30] shows a peak-like structure B and a shoulder A′ at 0.89 and 1.27 eV, respectively and have much larger values than the calculated ones. The measured σ spectrum by Rhee et al. [29] carries two peaks B and C at 0.99 and 4.1 eV, respectively with the overall magnitude close to our calculation. Our peak B and C seem to be shifted towards higher energies compared to Ref. [29]. The peak D has not been observed experimentally due to spectral limitations in these measurements. The experimental σ spectra are less rich in structures than the calculated spectrum. However, the general trend in the calculated and measured spectra appears to be consistent.

The part of the spectrum near the low energy end (~0 eV) shows a sharp increase of conductivity corresponding to intraband transitions in metals which have been accounted for by the supercell calculation. The intraband transitions in metals are usually approximated by the Drude model ($\sigma(\omega) = (\sigma_0/1 + i\omega\tau)$), where τ is the relaxation time. In this work, it is actually calculated using *ab initio* wave functions. From Fig. 4, we can also conclude that interband transitions in Ni_3Al start at about 0.5 eV. We have also checked that the use of a finer mesh of 35 *k*-points, as compared to 8 *k*-points for supercell calculations, modifies only the intensities of the peaks slightly but not their positions. Although it is well known that Ni_3Al is ordered at room temperature, here we introduce the disorder by arbitrary interchange the Ni and Al positions by design in order to study the effect disorder on the electronic structure of the alloy. We are not aware of any experimental data published on the disordered phase.

4. Results of the disordered phase

We next study the electronic structure and optical conductivity of the disordered phase of Ni_3Al and the results are compared with those of the ordered phase. We are not aware of any experimental data published on the disordered phase.

4.1. MD model construction

To construct models of the disordered alloy at various temperatures, we used a $4 \times 4 \times 4$ supercell and the experimental lattice constant of 3.568 Å [28]. Then, we arranged for purely substitutional disorder in the model by randomly interchanging the Ni and Al atoms to obtain the initial atomic positions for the disordered phase. Next, we performed molecular dynamics (MD) simulations to generate models at 300, 1000, 1400, and 1800 K using the embedded atom method (EAM) based potential functions. The EAM was proposed by Daw and Baskes [48], and has been a very effective method for metallic systems due to its enhanced accuracy and capability to describe low density defects such as free surfaces [49–51]. The key element for a successful simulation using EAM is to have well-tested and accurate potential functions. Several EAM potentials have been proposed for Ni_3Al (see [52] for a review), the best known of them being the potentials derived by Foiles and Daw [53], and Voter and Chen [54]. More recently, Y. Mishin [55] has developed the potential functions for the Ni–Al system and has successfully applied to investigate lattice properties of Ni_3Al, point defects, planar faults, as well as the γ and γ' fields on the Ni–Al phase diagram. We have adopted the potential functions by Y. Mishin to perform our MD simulation for the disordered Ni_3Al.

In present MD study, the NPT (constant number of atoms, pressure, and temperature) ensemble was used to simulate the heating process of the alloy. The temperature of the initial model was raised up to 2000 K, in temperature steps of 100 K after every 50,000 MD steps (i.e. about 5 ps). Fig. 1(b) shows a schematic unit cell of the disordered Ni_3Al alloy. The unit cell shown is one of the many possible cells among the whole disordered lattice and it does not necessarily repeat itself in building up the entire supercell. Fig. 5 shows the volume change against temperature during MD simulation. The change in volume is slow up to 1000 K, after which there is a rapid increase in volume as temperature increases. The region between 1600 K and 1800 K represents the range of phase change, in agreement with the experimental melting point of ~1658 K [56]. At 1800 K, the alloy is in the liquid phase.

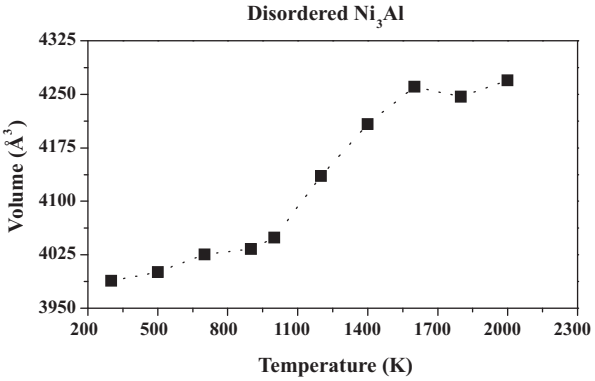

Fig. 5. Volume verses temperature plot for disordered Ni_3Al.

These disordered models for Ni_3Al from MD simulations are snapshots at various temperatures. The models can be considered as one of the possible frozen structures at a particular temperature. In order to calculate the electronic structure using *ab initio* method, these structures need to be further refined to achieve the minimum energy criteria. We used the Vienna *ab initio* simulation package (VASP) [57] to optimize the structures from MD simulation. VASP is based on DFT and uses plane waves as the basis functions for the construction of Bloch functions. It is an efficient and reliable method especially for the atomic relaxation and geometry optimization. To ensure sufficient accuracy, we have used a fairly high-energy cutoff of 400 eV. The Davidson block iteration scheme [58] was used for the optimization of the wave function. Ultra-soft Vanderbilt-type pseudopotentials [59] as supplied by Kresse and Hafner [60] have been adopted and only 1 *k*-point in the BZ is used. A relatively high accuracy for the ground state electronic convergence (10^{-5} eV) and a small tolerance for the ionic relaxation convergence (10^{-3} eV) were used. The VASP relaxations were performed with a fixed volume and fixed cell shape.

In an amorphous solid or disordered alloy, the structure is usually represented by the radial pair distribution function (RPDF). It describes the density of inter-atomic distances and is independent of orientation. When the RPDF of the initial model after VASP relaxation is broken down into Ni–Ni, Al–Al, and Ni–Al components it is clear that the greatest variability in initial position is derived from the Al atoms and that the Ni atoms tend to keep their crystalline configuration. The RPDF of disordered Ni_3Al at four different temperatures 0, 300, 1400, and 1800 K are shown in Fig. 6. At 0 K sharp peaks originated from the inter-atomic distances of the somewhat regular lattice sites are present. With the rise in temperature, this feature is quickly lost and peaks are broadened into very diffuse structures representing the disordered environment. However the strong non-symmetric peak positioned at approximately 2.5 Å remains at all temperatures representing the different types of the nearest neighbor (Ni–Al, Ni–Ni, and Al–Al) pairs. With the rise of temperature the intensity of this peak falls from 6.6 at 300 K to 5.85 at 1800 K. We also observe that the shape of this peak at 1400 K (before melting), and 1800 K (after melting) shows discernable differences. Beyond this strong peak, there is more broadening (and also more disordering) observed for the liquid phase.

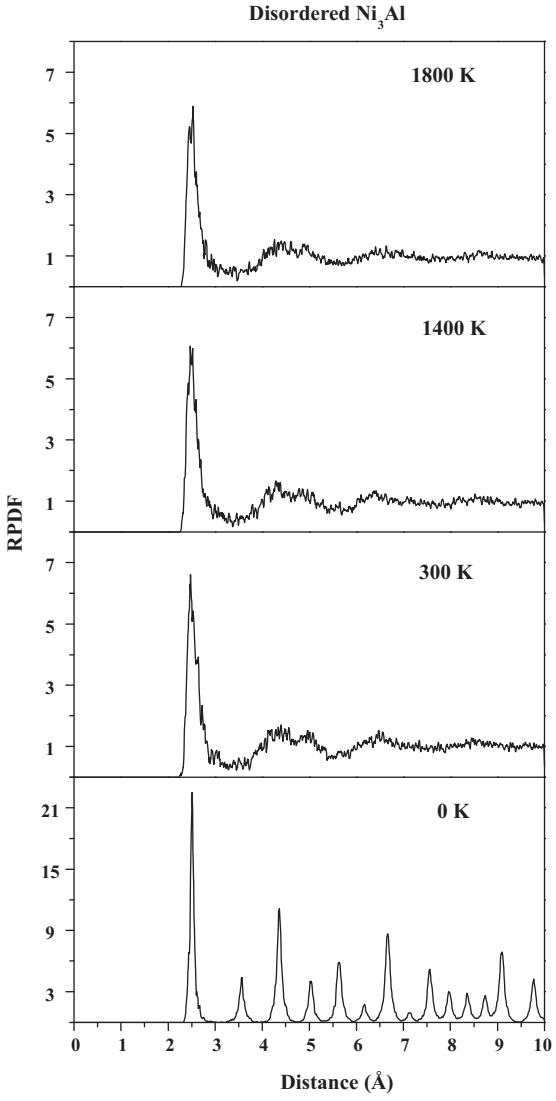

Fig. 6. Radial pair distribution function plots for the disordered Ni_3Al at various temperatures.

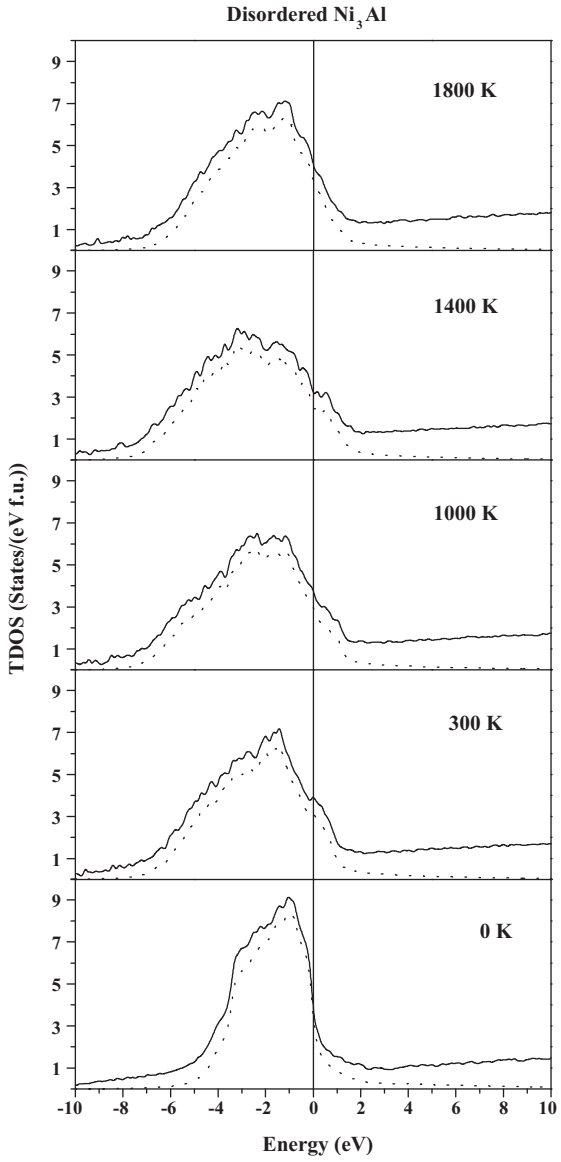

Fig. 7. TDOS spectra (solid curve) for disordered Ni_3Al at various temperatures. The dotted curve below the solid one represents the Ni-3d plot at the respective temperature. The Fermi level is taken as zero energy.

4.2. Electronic structure

The electronic structure of the disordered phase of the Ni_3Al at different temperatures was calculated in the same manner as the ordered phase described in Section 3. The calculated TDOS of the disordered Ni_3Al at various temperatures are shown in Fig. 7 as solid lines. These spectra exhibit fewer structures on the whole as compared to the ordered phase. The dotted line below the solid line represents the projected PDOS of Ni-3d orbitals which clearly dominates the TDOS at all temperatures, even for the liquid phase at 1800 K. The contribution from Al to these spectra is very small as was observed for the ordered phase. The main peak in the TDOS spectra for $T = 0$, 300, 1000, 1400, and 1800 K models are at −1.00, −1.41, −2.33, −3.20, and −1.15 eV, respectively below the Fermi level E_F. The peak structure shifts to lower binding energy from the Fermi level as temperature increases. However, at the liquid phase ($T = 1800$ K), this peak shifts back towards E_F, indicating a rather different electronic interaction before and after melting. For each temperature the TDOS at the Fermi level, $N(E_F)$, is listed in Table 2. It shows that $N(E_F)$ drops as T increases but increases at the liquid temperature of 1800 K. The same trend exists for the TDOS peak intensity. It drops steadily from 9.14 states/(eV formula unit) at 0 K to 6.25 states/(eV formula unit) at 1400 K, but increases to 7.12 states/(eV formula unit) at the liquid temperature.

Fig. 8 shows the calculated LI of the ordered and disordered Ni_3Al according to Eq. (1). The generally accepted notion regarding electron localization in a disordered solid such as an amorphous semiconductor is that the states at the band edges are localized and those at the centre of the bands are delocalized. In metallic

Table 2
Calculated results for DOS at the Fermi level in Ni_3Al.

Model used	$N(E_F)$ [states/(eV formula unit)]
Ordered	
Primitive cell	5.82
Supercell	5.84
Disordered	
0 K	3.97
300 K	3.91
1000 K	3.78
1400 K	3.25
1800 K	4.14

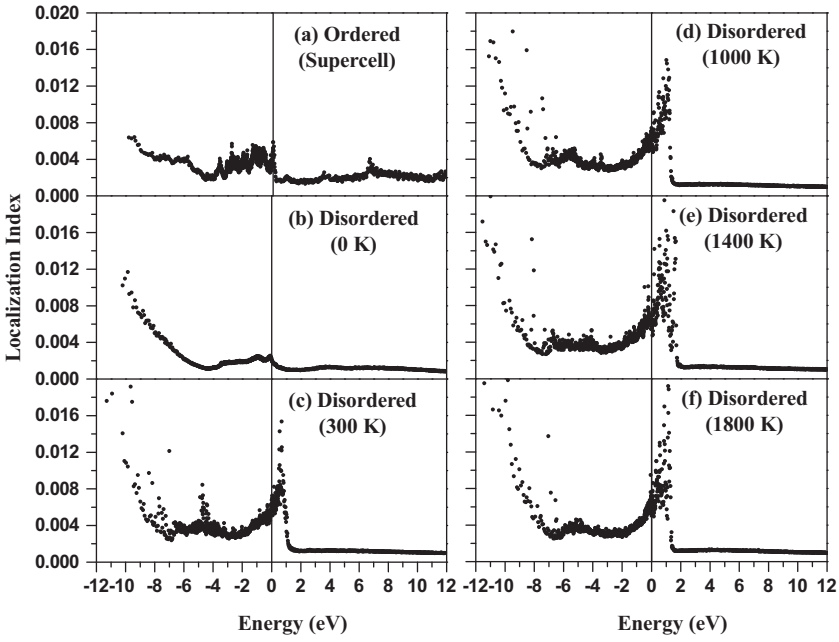

Fig. 8. Localization index (LI) plots for ordered (a) and disordered (b–f) Ni_3Al.

systems, this notion is less clear since electrons in metals are supposed to be mobile (i.e. totally delocalized), although d-orbitals are usually more localized than s- or p-orbitals. In the context of the present work, we will focus on the electron states within a few eV of the Fermi level where Ni-3d states dominate. It is shown that their relative degree of localization can be influenced by the potential fluctuations introduced by disorder and temperature effects. States near E_F in the ordered phase are slightly more localized than those in the disordered phase at 0 K. This is due to the fact that in the ordered crystalline phase, the d-orbitals of Ni (xx, yy, zz, x^2-y^2, r^2-3z^2) with specific interactions with the nearest neighbor Al atoms form symmetry related bands (see Fig. 2), some of them are relatively more localized (flat bands). In the disordered phase at zero K, Ni–Ni and Al–Al interactions are now present and there are more varieties of orbital interactions which make the electron states somewhat delocalized. As the temperature is increased, there is a dramatic increase in the LI of the states within about 1.5 eV of the Fermi level (see Fig. 8(c)–(f)). Obviously, the positional disorder from the thermal fluctuations causes substantial localization in contrast to the $T = 0$ K case where substitutional disorder alone induces delocalization. This applies only to states dominated by d-orbitals. On the other hand, the states above 1.5 eV are completely delocalized since their wave functions are composed mostly of s- and p-orbitals.

The calculated Q^* data of disordered Ni_3Al at different temperatures and the associated charge transfer are listed in Table 1. The net charge gained by the Ni atoms increases with temperature from 0.123 electrons/atom at 0 K to 0.156 electrons/atom at 1400 K as shown in Fig. 9. After melting (1800 K) the liquid phase Ni atoms show a decreased average gain of only 0.130 electrons/atom. Al atoms lose 0.390 electrons/atom on average in the liquid phase. This is another indication of the difference in the electronic structure between the solid and the liquid phase.

4.3. Optical conductivity (σ)

The optical conductivities of the disordered models of Ni_3Al are displayed in Fig. 10. At $T = 0$ K, σ has a strong peak α at 4.96 eV and a weak peak β at 2.1 eV. With the rise of temperature, α broadens and shifts towards a high energy value (6.47 eV) for the 300 K model and to 6.62 eV for the 1400 K model. In the liquid phase this peak shifts back to 5.83 eV indicating rather different electronic states in the two phases. At the energy close to 0 eV, σ increases rapidly accounting for the same metallic conductivity as in the crystalline case and in all metallic systems. Such results can only be achieved if a sufficiently large supercell is used for the calculation.

It is interesting to compare the optical conductivity of the ordered phase of Ni_3Al (Fig. 4) with that of the disordered phase at 0 K (Fig. 10, lowest panel) using the supercells of the same size. In the ordered phase, the spectrum is rich in structures as discussed in Section 3. The spectrum for the disordered phase is completely different and much simpler with a major peak α and a weaker peak β. In the disordered phase, the inter-atomic pairs (Ni–Al, Ni–Ni, and Al–Al) are distributed randomly and gave very different RPDF and LI as discussed earlier. This resulted in rather different electronic states, both occupied and unoccupied, and are responsible for the very different optical conductivities. Unfortunately, we cannot locate any experimental or theoretical data that can confirm our calculated results.

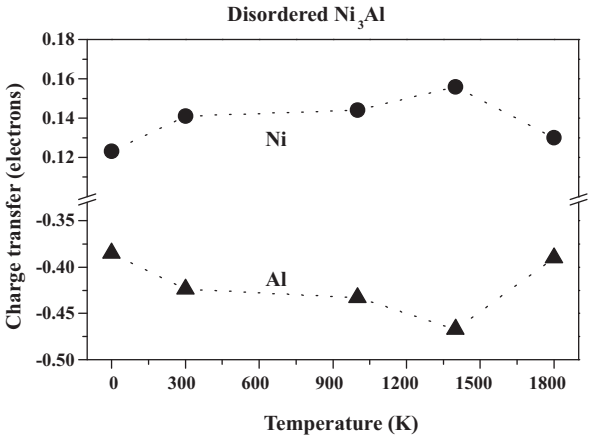

Fig. 9. Plots for charge transfer trend occurring in Ni and Al atoms in disordered Ni_3Al.

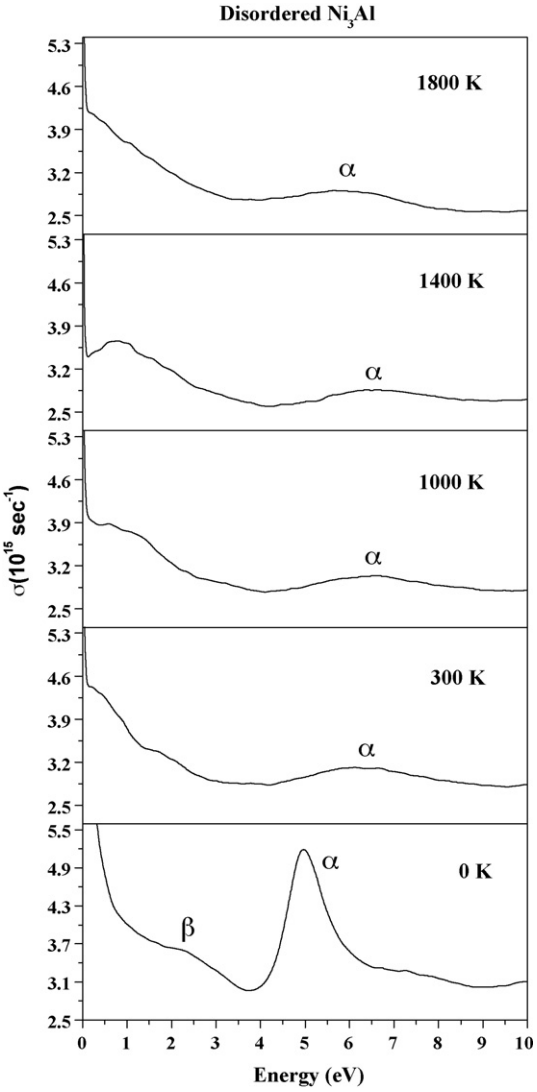

Fig. 10. Optical conductivity spectra of disordered Ni_3Al at various temperatures.

5. Conclusions

We have performed electronic structure and optical conductivity calculations for both the ordered ($L1_2$) as well as the disordered (fcc solid solution) phases of the Ni_3Al using the first-principles OLCAO method based on a supercell approach. For the disordered phase, models of the alloys at different temperatures were obtained using the MD simulation followed by *ab initio* relaxation. Our calculations show that the major contribution to the TDOS spectra for both the ordered and disordered phases is from the Ni-3d orbitals with the Fermi level cuts at the steeper side of the TDOS spectra. The TDOS spectra in the disordered phase contain fewer structures than that in the ordered phase and look more like a broadened version of the ordered DOS. However, the electron states in the disordered phase are fundamentally different from that of the ordered phase. The LI of the disordered phase at various temperatures shows that the states are highly localized above the Fermi level up to 2.0 eV, while the higher conduction band states (above 2.0 eV) are completely delocalized. The calculation of effective charges shows a net charge transfer from Al to Ni in both phases. The electronic structure results also show a substantial difference in the liquid phase (at 1800 K) compared to the solid phase.

The optical conductivity calculation for the ordered Ni_3Al shows an overall good agreement with the experimental spectra, even though there are large variations among the current experimental data. In the disordered phase, the optical conductivity curve is much simpler in structure and is very different from the ordered phase. In both cases, σ increases rapidly as the transition energy approaches to zero eV characteristic of metallic systems involving intraband transitions. This is achieved by using a sufficiently large supercell. In most calculations, this part of the optical conductivity is always approximated by the Drude term with an adjustable parameter to fit the experimental data if available. In the present work, we demonstrate that the intraband optical conductivities can be calculated using *ab initio* method in the supercell approach. The success of this approach critically depends on the efficiency and accuracy of the underlying method for the electronic structure theory such that the computations are not prohibitive when large supercells are used.

Finally, we conclude that this work demonstrates the importance of detailed computational studies for disordered systems where experimental data may be lacking or difficult to perform. As mentioned in the introduction, there are major applications for Ni_3Al alloys at high temperature where disordered phases invariably exist; fundamental understanding of their electronic structure and optical properties can accelerate their use in potential new applications. The present study does not include the spin-dependent magnetic ordering in the calculation due to prohibitive computational costs for large supercells. Future investigations will extend to such studies. It is also possible to study the compositional dependence of the electronic structure and optical properties of non-stoichiometric compositions of the Ni_3Al alloy using the same supercell approach.

Acknowledgements

Altaf Hussain is thankful to the Department of Physics, University of Missouri-Kansas City (UMKC), for providing access to the computational resources and providing local hospitality. He is also thankful to the Higher Education Commission (HEC) of Pakistan, for supporting financially and making it possible for him to work at UMKC (USA).

References

[1] G. Welsch, P.D. Desai, Oxidation and Corrosion of Intermetallic Alloys, Purdue Research Foundation, West Lafayette, 1996, p. 167.
[2] N.S. Stoloff, V.K. Sikka, Physical Metallurgy and Processing of Intermetallic Alloys, Chapman and Hall, New York, 1996, p. 561.
[3] B.H. Kear, C.T. Sims, N.S. Stoloff, J.H. Westbrook, Ordered Alloys-Structural Applications and Physical Metallurgy, Claitors Pub. Div., Baton Rouge, 1970, p. 1.
[4] C.C. Koch, C.T. Liu, N.S. Stoloff, MRS Symp. Proc. (1985) 39.
[5] N.S. Stoloff, C.C. Koch, C.T. Liu, O. Izumi, MRS Symp. Proc. (1987) 81.
[6] C.T. Liu, A.I. Taub, N.S. Stoloff, C.C. Koch, MRS Symp. Proc. (1989) 133.
[7] L.A. Johnson, D.P. Pope, J.O. Stiegler, MRS Symp. Proc. (1991) 213.
[8] I. Baker, R. Darolia, J.D. Whittenberger, M.H. Yoo, MRS Symp. Proc. (1993) 288.
[9] V.K. Sikka, J.T. Mavity, K. Anderson, Mater. Sci. Eng. A 153 (1992) 712.
[10] V.K. Sikka, S.C. Deevi, J.D. Vought, Adv. Mater. Process 147 (1995) 29.
[11] C.G. McKamey, J.H. DeVan, P.F. Tortorelli, V.K. Sikka, J. Mater. Res. 6 (1991) 1779.
[12] T. Czeppe, S. Wierzbinski, Int. J. Mech. Sci. 42 (2000) 1499.
[13] R. Arroyave, D. Shin, Z.K. Liu, Acta Mater. 53 (2005) 1809.
[14] G. Karin, H. Luo, D. Feng, C. Li, J. Iron Steel Res. Int. 14 (2007) 21.
[15] V.K. Sikka, M.I. Santella, P. Angelini, J. Mengel, R. Petrusha, A.P. Martocci, R.I. Pankiw, Intermetallics 12 (2004) 837.
[16] M. Krasnowski, A. Antolak, T. Kulik, J. Alloys Compd. 434–435 (2007) 344.
[17] Y. Wang, Z.K. Liu, L.Q. Chen, Acta Mater. 52 (2004) 2665.
[18] V.K. Sikka, S.C. Deevi, S. Viswanathan, R.W. Swindeman, M.L. Santella, Intermetallics 8 (2000) 1329.
[19] P.B. Da Silva-Maia, F. Velasco, N. Anton, C.E. Da Costa, W.C. Zapata, Adv. Perform. Mater. 6 (1999) 117.
[20] J.Q. Su, M. Demura, T. Hirano, Acta Mater. 51 (2003) 2505.
[21] D.P. Pope, S.S. Ezz, Int. Metals Rev. 29 (1984) 136.
[22] N. Buis, J.J.M. Franse, P.E. Brommer, Physica B + C 106 (1981) 1.
[23] S.K. Dhar, K.A. Gschneidner, Phys. Rev. B 39 (1989) 7453.
[24] N.R. Bernhoeft, G.G. Lonzarich, P.W. Mitchell, D. McK Paul, Phys. Rev. B 28 (1983) 422.

[25] T.I. Sigfusson, N.R. Bernhoeft, G.G. Lonzarich, J. Phys. F 14 (1984) 2141.
[26] F. Wallow, G. Neite, W. Schroer, E. Nembach, Phys. Status Solidi A 99 (1987) 483.
[27] P.A.M. van der Heide, J.J.M. Buiting, L.M. ten Dam, L.W.M. Schreurs, R.A. de Groot, A.R. de Vroomen, J. Phys. F: Met. Phys. 15 (1985) 1195.
[28] J.Y. Rhee, B.N. Harmon, D.W. Lynch, Phys. Rev. B 55 (1997) 4124.
[29] J.Y. Rhee, Y.V. Kudryavtsev, Y.P. Lee, Phys. Rev. B 68 (2003) 045104.
[30] L.S. Hsu, Y.K. Wang, J. Alloys Compd. 377 (2004) 29.
[31] M.A. Khan, A. Kashyap, A.K. Solanki, T. Nautiyal, S. Auluck, Phys. Rev. B 48 (1993) 16974.
[32] M.H. Enayati, Z. Sadeghian, M. Salehi, A. Saidi, Mater. Sci. Eng. A (2004) 809.
[33] D.D. Fontaine, J. Althoff, D. Morgan, M. Asta, S. Foiles, A. Quong, D. Johnson, MRS Symp. Proc. (1998) 175.
[34] A. van de Walle, G. Ceder, U.V. Waghmare, Phys. Rev. Lett. 80 (1998) 4911.
[35] S. Lay, A.R. Yavari, Mater. Sci. Form. (1995) 179.
[36] B. Fultz, L. Anthony, L.J. Nagel, R.M. Nicklow, S. Spooner, Phys. Rev. B 52 (1995) 3315.
[37] F. Cardellini, V. Contini, G. Mazzone, Scripta Metall. Mater. 32 (1995) 641.
[38] W.Y. Ching, J. Am. Ceram. Soc. 73 (1990) 3135.
[39] R. Magri, S.H. Wei, A. Zunger, Phys. Rev. B 42 (1991) 11388.
[40] S. Aryal, P. Rulis, W.Y. Ching, Am. Mineral. 93 (2008) 114.
[41] H. Yao, L. Ouyang, W.Y. Ching, J. Am. Ceram. Soc. 90 (2007) 3194.
[42] S. Yang, L. Ouyang, J.M. Phillips, W.Y. Ching, Phys. Rev. B 73 (2006) 165407.
[43] L. Ouyang, P. Rulis, W.Y. Ching, M. Slouf, G. Nardin, L. Randaccio, Spectrochimica Acta A 61 (2005) 1647.
[44] J. Chen, L. Ouyang, W.Y. Ching, Acta Mater. 53 (2005) 4111.
[45] W.Y. Ching, Phys. Rev. Lett. 46 (1981) 607.
[46] R.S. Mulliken, J. Am. Chem. Soc. 23 (1955) 1833;
R.S. Mulliken, J. Am. Chem. Soc. 23 (1955) 1841.
[47] D. Greenwood, Proc. Phys. Soc. 71 (1958) 585.
[48] M.S. Daw, M.I. Baskes, Phys. Rev. B 29 (1984) 6443.
[49] M.S. Daw, S.M. Foiles, M.I. Baskes, Mater. Sci. Rep. 9 (1993) 251.
[50] A.F. Voter, Intermetallic Compounds: Principles and Practice, 1, John Wiley and Sons Ltd, 1995, p. 77.
[51] E. Ahmed, J.I. Akhter, M. Ahmad, Comput. Mater. Sci 31 (2004) 309.
[52] M.I. Baskes, Acta Metall. Sin. 8 (1995) 287.
[53] S.M. Foiles, M.S. Daw, J. Mater. Res. 2 (1987) 5.
[54] A.F. Voter, S.P. Chen, MRS Symp. Proc. (1987) 175.
[55] Y. Mishin, M.J. Mehl, D.A. Papaconstantopoulos, Phys. Rev. B 65 (2002) 224114.
[56] R. Ravelo, J. Aguilar, M. Baskes, J.E. Angelo, B. Fultz, B.L. Holian, Phys. Rev. B 57 (1998) 862.
[57] G. Kresse, J. Furthmuller, Comp. Mater. Sci. 6 (1996) 15;
G. Kresse, J. Furthmuller, Phys. Rev. B 54 (1996) 11169.
[58] N. Soga, J. Geophys. Res. 72 (1967) 4227.
[59] D. Vanderbilt, Phys. Rev. B 41 (1990) 7892.
[60] G. Kresses, J. Hafner, J. Phys.: Condens. Matter 6 (1994) 8245.